Journal of Alloys and Compounds, 848 (2020) 156566.
https://doi.org/10.1016/j.jallcom.2020.156566

Milling effects on the distribution of Curie temperatures and magnetic properties of Ni-doped $La_{0.7}Ca_{0.3}MnO_3$ compounds

A.F. Manchón-Gordón[1], A. Gómez[2], J.J. Ipus[1], J.S. Blázquez[*1], C.F. Conde[1], A. Conde[1]

[1]*Dpto. Física de la Materia Condensada, ICMSE-CSIC, Universidad de Sevilla, P.O. Box 1065, 41080 Sevilla, Spain*
[2]*Grupo GIIEN, Institución Universitaria Pascual Bravo. Calle 73 No. 73A – 226. Medellín 050034. Colombia*
[*]*The corresponding author e-mail:* jsebas@us.es

ABSTRACT: A systematic study of the magnetic and magnetocaloric properties around the ferromagnetic-paramagnetic phase transition temperature have been carried out on $La_{0.7}Ca_{0.3}Mn_{1-x}Ni_xO_3$ (x = 0, 0.02, 0.07, 0.10) compounds synthesized by ball milling from oxides and pure Ni. The order of the transition, analyzed by the Banerjee's criterion and the field dependence of the magnetic entropy change, was found to be of second order for all the studied compositions. The existence of small traces of β-MnO_2 phase and the distortions produced during the milling process may induce a competition character of the ferromagnetic and the antiferromagnetic interactions at low fields and motivate the existence of a distribution of Curie temperatures. Once the antiferromagnetic contributions are avoided, the parameters of the distribution, the average Curie temperature $\overline{T_C}$ and the broadening of the distribution ΔT_C, have been obtained from the analysis of the approach to saturation curves and the magnetocaloric effect.

KEYWORDS: LCMO manganites, ball milling, Curie temperature distribution, magnetocaloric effect

1. INTRODUCTION

The magnetic refrigeration at temperatures close to room temperature, taking advantage of the magnetocaloric effect (MCE), has been considered for future developments in cost-effective new technologies due to its possibilities for saving energy and mitigating environmental problems [1]. In this frame, perovskite manganites with a general formula $RE_{1-x}A_xMnO_3$ (RE is a trivalent rare earth element and A is a divalent or a

monovalent alkaline element) have attracted considerable attention thanks to their interesting magnetic and electronic properties in addition to their technological potential applications [1-3]. Among the studied lanthanum manganites, $La_{1-x}Ca_xMnO_3$ (LCMO) compounds have received particular attention because of their very rich physical phenomenology. For example, they can exhibit a first-order magnetic phase transition (FOPT) when x=0.3 and can offer giant MCE tunable around room temperature [3]. The properties of these compounds are strongly dependent on both coupling between the trivalent (Mn^{3+}) and tetravalent (Mn^{4+}) ions [4] and electron-phonon coupling arising from the Jahn-Teller effect [5].

The influence of the Mn substitution by other transition metals on the crystal structure and magnetic properties of $La_{1-x}Ca_xMnO_3$ compounds is very interesting in order to optimize their properties and, particularly, to tune the Curie temperature [6-9]. In these manganites, the substitution of La^{3+} by Ca^{2+} generates Mn^{4+} ions which ferromagnetically couple to neighbor Mn^{3+} ions, via double-exchange interactions [10]. For Ni doped $La_{1-x}Ca_xMnO_3$ compounds, it has been pointed out that the Mn substitution by a small amount of Ni could change the magnetic and transport properties without changing significantly their crystal structure [6-9]. Basically, increasing Ni-doping content reduces the Curie temperature of the ferromagnetic-paramagnetic phase transition due to weakened double-exchange interactions.

Although there is a significant number of studies on Ni doped lanthanum manganites, there is a lack of information related to the effect of the use of high-energy ball milling for synthesizing these compounds. In fact, the properties of these compounds vary with the production method. In this context, several works can be found in the literature studying the effect of production methods on microstructural, electrical and magnetic properties of different perovskite compositions [11-13]. Although the solid state

reaction method is the most used to obtain manganites, ball milling technique from simple oxides has been successfully used to synthesize manganites with perovskite structure [12, 14, 15]. During the milling, the powders are continuously exposed to different phenomena, such as fracture and cold welding, which define the microstructure of the final products, affecting the magnetic properties of the samples produced by this technique. For example, in the case of MCE, a general decrease in the peak value of the magnetic entropy change as well as a large broadening of its thermal dependence have been reported [12, 16]. This is generally associated to the existence of a non-negligible distribution of transition temperatures [16-18]. In doped systems, the presence of the doping atom can also lead to compositional disordering and thus to enhancement of the distribution of transition temperatures. Recently, a procedure to obtain the average Curie temperature and the broadening of such distributions from the analysis of the approach to the saturation curves and MCE has been reported, successfully applied to amorphous metals and intermetallics [18, 19]. In this study, this procedure has been applied to a series of LCMO doped with nickel, $La_{0.7}Ca_{0.3}Mn_{1-x}Ni_xO_3$ (x=0, 0.02, 0.07, 0.10), produced by high-energy ball milling. The magnetic behavior has been analyzed and the results have been compared with those of samples synthetized by other methods.

2. EXPERIMENTAL

$La_{0.7}Ca_{0.3}Mn_{1-x}Ni_xO_3$ (x=0, 0.02, 0.07, 0.10) samples were synthesized via mechanical milling at room temperature in air using a Fritsch Pulverisette 4 Vario-Planetary Mill with hardened steel balls and stainless steel vials. MnO_2, La_2O_3, CaO and Ni powders were used as precursor materials. The ball to powder weight ratio was 10:1. The vial frequency Ω = 250 rpm was used for samples with x=0 and x=0.10 until 70 h of milling.

For larger times of milling, Ω = 350 rpm was used to speed up the process. In the case of the samples with x=0.02 and 0.07, taking into account the acquired knowledge on the previous samples, Ω = 350 rpm was used during all the milling process. In order to make the different milling easily comparable, an equivalent time approach, $t_{eq} = t\left(\frac{\Omega}{\Omega_0}\right)^3$ [20], was used for scaling the ball milling processes in planetary mills, where Ω_0 is a reference frequency and Ω the milling frequency of the experiment. In this study the highest frequency used in our experiments has been used as reference frequency, i.e. Ω_0= 350 rpm. The maximum equivalent time of milling was 155.5 h. To prevent the overheating of the vials, the experiments were carried out by alternating 30 min of milling with 30 min at rest.

The structure of the synthesized samples was investigated via X-ray diffraction (XRD), with a Cu-Kα radiation source (λ=1.5406 Å) in a Bruker D8 I diffractometer. Rietveld refinements were performed by TOPAS software (Version 6).

The magnetic properties were measured as a function of the temperature, using a Lakeshore 7407 vibrating sample magnetometer and a maximum applied field of $\mu_0 H$= 1.5 T. The saturation magnetization at zero field, M_S, and paramagnetic susceptibility, χ_p, were obtained by fitting the experimental high-field magnetization curve to the law of approach to saturation [21]. The magnetic entropy change ΔS_M was calculated from isothermal magnetization curves, using the Magnetocaloric Effect Analysis Program [22] available from Lakeshore Cryotronics, Inc.

3. RESULTS and DISCUSSION

Figure 1a shows the XRD patterns taken at room temperature for the undoped alloy after the indicated equivalent milling times, ranging from 0 to 155.5 h. The pattern of the powder milled during 0.4 h shows the peaks corresponding to the starting oxides: La_2O_3, MnO_2 and CaO. The low intensity of the peaks of the latter oxide is in agreement with the development of the intermediate La_2CaO_4 phase. The intensity of the peaks of the starting oxides decreases with the increase of milling time and, after t_{eq}=6.6 h, only peaks ascribed to the MnO_2 phase can be observed. After t_{eq}=10.2 h, peaks ascribed to $La_{0.7}Ca_{0.3}MnO_3$ (LCMO) phase are detected, and their intensity progressively increases with the increase of t_{eq}. At larger equivalent milling times, the intensity of the peaks belonging to original MnO_2 phase decreases, although small traces can be found even after t_{eq}=155.5 h along with the peaks of the target LCMO phase. Similar results have been obtained for all the Ni content studied alloys. Figure 1b shows the XRD diffraction patterns of the studied samples at t_{eq}=155.5 h, the maximum milling time analyzed in this study. A final value of crystal size ~15 nm for the LCMO phase is achieved for all the studied compounds.

Figure 2 shows the temperature dependence of magnetization taken at 0.1 T for $La_{0.7}Ca_{0.3}Mn_{1-x}Ni_xO_3$ (x=0, 0.02, 0.07, 0.10) samples at t_{eq}=155.5 h. A decrease of the magnetization is observed due to the Curie transition of the samples. Curie temperature T_C can be roughly determined by identifying the temperature at which the temperature derivative of the magnetization $\frac{dM}{dT}$ shows a minimum, T_{inf} (see inset Fig. 2). However, the obtained value of T_{inf} is field dependent and the temperature range at which $\frac{dM}{dT}$ curves deviate from zero is large. The latter characteristic is consistent with the existence of a distribution of Curie temperatures, typical of compounds produced by mechanical milling [12, 16]. For that reason, a more realistic value of Curie temperature

will be obtained below after a detailed analysis assuming the presence of a Gaussian Curie temperatures distribution.

The Banerjee's criterion has been used to determine the order of the magnetic phase transition. Following this criterion, if the plot H/M vs. M^2 has a positive slope, the magnetic transition corresponds to a second-order transition, while if a negative slope is found, the system experiences a first-order transition. The results of this analysis for the undoped sample at t_{eq}=155.5 h are shown in Figure 3. It can be seen that all the curves present a positive slope, indicating the second order character of its magnetic transition. Similar results have been obtained for the samples with x=0.02, 0.07 and 0.10 (not shown). Although attending to Banerjee's criterion our samples present a second-order phase transition, it has to be noted that most mixed-valence manganites are associated with first-order magnetic transition [1]. However, the character of the transition is very sensitive to the production process. In fact, it has been found in $La_{0.7}Ca_{0.3}MnO_3$ compounds that the type of magnetic phase transition changes from first to second-order with the decrease in the particle size [23]. Similar effects concerning the change from first to second-order as the mean grain size decreases has also been observed in other systems [24, 25]. Furthermore, changes in the character of the magnetic phase transition from first to second-order have been reported in Ni-Fe-Ga based magnetic shape memory alloys via mechanical treatments [26].

Isothermal magnetization curves were recorded to evaluate the magnetic entropy change in the studied samples around the transition temperature of each system. Figure 4 shows the magnetic entropy change from zero field up to 1.5 T as a function of temperature for the studied samples at t_{eq}=155.5 h. Although there is no monotonous behavior of ΔS_M with Ni content (the maximum entropy changes observed are -0.89, -0.77, -0.70 and -0.95 $Jkg^{-1}K^{-1}$ at 1.5 T for x=0, 0.02, 0.07 and 0.10, respectively), it has been

reported that ΔS_M values decrease with Ni doping [8]. The milling process could lead to a stronger disorder in the structure of the sample with higher Ni content, altering the magnetic interactions of the compounds, and that could explain the change in the tendency. In fact, values for x=0, 0.02 and 0.07 are in good agreement with those found in the literature for the same compounds produced by auto-combustion method [8] and the undoped sample synthesized by sol-gel method [23]. It is worth noticing that, in both cases, the mean size of the particles was similar (about 20 and 50 nm, for the samples produced by auto-combustion and sol-gel method, respectively). In fact, significant differences in ΔS_M values, even larger than an order of magnitude, can be found in the same compound for different particle size [23]. Generally, a decrease of the crystal size in manganite compounds leads to a decrease of the MCE response due to the change from first to second-order transition.

In recent studies, the field dependence of the magnetic entropy change has been shown to be more sensitive than the Banerjee's criterion to determine the order of the magnetic transition [27]. This field dependence, assuming a zero starting field, can be expressed as:

$$|\Delta S_M(T,H)| = a(T)H^{n(T,H)} \quad (1)$$

For single phase systems with a second-order phase transition, exponent n is field independent in three regions: well below the Curie temperature (n=1), well above the transition (n=2) and at Curie temperature, where n is related with the critical exponents [28]. Moreover, more recently it has been reported that the exponent n presents a maximum of n>2 for temperatures above transition only for first-order thermomagnetic phase transitions [27]. Inset of Figure 4 shows the temperature dependence of the exponent n characterizing the field dependence of ΔS_M. The obtained values agree with

those expected for systems that present a second-order magnetic transition and the conclusions derived from the Banerjee's criterion (see Fig.3).

$M(T)$ and magnetic entropy change $\Delta S_M(T)$ curves show a broad transition instead of the sharper and better defined transition expected for a theoretically pure system. Indeed, the typical compositional inhomogeneities of the samples produced by ball milling could lead to a distribution of some characteristic parameters. The knowledge of the parameters characterizing those distributions helps to obtain a more realistic description of the behavior of the samples. Recently, we have proposed a method to obtain the parameters of a distribution of Curie temperatures using the differences between the inflection point T_{inf} of the saturation magnetization at zero field curves $M_S(T)$, the peak temperature of the paramagnetic susceptibility T_{pk}^{χ} and the peak temperature of the maximum entropy change T_{pk}^{MCE} [18, 19]. Furthermore, it has been found that the estimated critical exponents of polycrystalline $La_{0.7}Ca_{0.3}Mn_{1-x}Ni_xO_3$ (x=0, 0.02, 0.07 and 0.10) are in agreement with the mean-field model [29]. In this case, the average Curie temperature $\overline{T_C}$ and the broadening of the distribution ΔT_C can be obtained combining the three following equations (in fact, only two of them should be needed) [18,19]:

$$T_{inf} - \overline{T_C} = -0.732(6)\Delta T_C, \quad (2)$$

$$T_{pk}^{\chi} - \overline{T_C} = 0.502(23)\Delta T_C - 0.0039(7)\Delta T_C^2, \quad (3)$$

$$T_{pk}^{MCE} - \overline{T_C} = -0.658(8)\Delta T_C. \quad (4)$$

The law of approach to saturation has been used to obtain the values of the M_S and the paramagnetic susceptibility χ_p [21]:

$$M = M_S\left(1 - \frac{a}{H} - \frac{b}{H^2}\right) + \chi_p H. \quad (5)$$

Figure 5 shows the $M_S(T)$ and $\chi_p(T)$ values from fitting the experimental magnetization at high field ($\mu_0 H$> 1 T) for the studied alloys at t_{eq}=155.5 h. $M_S(T)$ continuously decreases with the increasing temperature due to the progressive change from the ferromagnetic to paramagnetic behavior of the samples. The difference between the peak temperatures of χ_p and dM_S/dT is, in mean field approach, an evidence of the presence of a distribution of transition temperatures (see equations 2 and 3).

The parameters of the Curie temperature distribution, $\overline{T_C}$ and ΔT_C, can be obtained by combining Eqs. 2, 3 and 4 and the experimental results of Fig. 4 and 5. Using Eqs. 2 and 3, $\overline{T_C}$ = 139, 134, 139 and 154 K for x=0, 0.02, 0.07, 0.10, respectively, and ΔT_C =12 K, independently of the composition (see Table 1). However, comparison of Eqs. 2 and 4 yields T_{inf}<T_{pk}^{MCE}, while the experimental values show that T_{pk}^{MCE}<T_{inf}. In fact, magnetic entropy change is obtained as:

$$\Delta S_M(T) = \mu_0 \int_{H_{min}}^{H_{max}} \left.\frac{dM}{dT}\right|_H dH, \quad (6)$$

where $\Delta S_M(T)$ is obtained as the sum of dM/dT at a fixed H and the highest term in each sum corresponds to the peak value of $\left.\frac{dM}{dT}\right|_H$. In particular, T_{inf} corresponds to the temperature at which the temperature variation of the magnetization at zero field is maximum (maximum $\left.\frac{dM}{dT}\right|_{H=0}$). However, as T_{pk}^{MCE}<T_{inf}, this demands that $\left.\frac{dM}{dT}\right|_H$ for $H > 0$ must be found at temperatures below T_{inf} (i.e. the magnetic field shifts the inflection point to lower temperatures). This atypical result has also been found in Sr doped $La_{0.7}Ca_{0.3}MnO_3$ compounds produced by high-energy ball milling, where the substitution of Ca^{2+} by Sr^{2+} increases the differences between T_{pk}^{MCE} and T_{inf} [30].

To elucidate the reason why this is observed, the field dependence of the dM/dT curves has been studied. It is worth mentioning that whereas T_{inf} was obtained after an extrapolation of high field behavior of the magnetization curves, ΔS_M shown in Figure 4 takes into account magnetization curves from zero field to 1.5 T. Figure 6 shows, as an example, the temperature dependence of magnetization at different magnetic fields displayed for the undoped studied manganite at t_{eq}=155.5 h along with the $M_S(T)$ curve obtained from the fitting of the law of approach to saturation. Inset shows the inflection point as a function of the applied magnetic field, $T_{inf}^{H}(H)$, along with T_{inf} from approach to saturation (indicated in red at zero field). It can be observed that the inflection temperature of the $M_S(T)$ curve, T_{inf}, is higher than the inflection temperatures obtained for fields below 1 T. Similar results can be found for the doped samples studied here. To explore the evolution of the inflection point as a function of the field in the frame of Weiss model, $T_{inf}^{H}(H)$, simulations of the Brillouin function have been performed assuming a Gaussian distribution of Curie temperatures with ΔT_C=12 K and $\overline{T_C}$=140 K. The plot of the simulated $T_{inf}^{Weiss}(H)$ is also shown in the inset of figure 6, where it can be seen that T_{inf} from the approach to saturation analysis is in agreement with the simulated curves in the frame of Weiss model. This confirms that the results obtained from the approach to saturation analysis are consistent and avoid the atypical effects observed at low magnetic fields.

Weiss model was also used to simulate $\Delta S_M(T)$ curves obtained for different minimum magnetic field H_{min} up to 1.5 T and assuming ΔT_C=12 K and $\overline{T_C}$=140 K (Figure 7a). It can be observed that the maximum value of $\Delta S_M(T)$ continuously decreases with H_{min} but changes in T_{pk}^{MCE} are ≤2 K in the showed range (see inset in Figure 7a). As mentioned above, the ΔS_M data showed in Figure 4 correspond to a field range from

zero field up to1.5 T, while $M_S(T)$ and $\chi_p(T)$ curves were obtained considering only the data for $\mu_0 H$>1 T, where the saturation of the magnetization is achieved. Therefore, in order to avoid the deviations from the Weiss predictions found at low fields, the magnetic entropy change as a function of the temperature has been analyzed, for all studied samples, for $\mu_0 H_{min}$=1 T and $\mu_0 H_{max}$=1.5 T (Figure 7b), i.e. in the field range used for the approach to saturation used in the fitting. A clear shift of T_{pk}^{MCE} to higher temperatures with respect to the results shown in Figure 4 can be observed and the predicted T_{inf}<T_{pk}^{MCE} behavior is recovered.

In order to be consistent with the field range used in the analysis of approach to saturation, the equation of T_{pk}^{MCE} shown in Eq. 4, calculated for the field range 0<$\mu_0 H$<1 T [18,19], has to be modified to a new equation defined for the field range 1<$\mu_0 H$<1.5 T (R^2=0.997):

$$T_{pk}^{MCE} - \overline{T_C} = -0.620(12)\Delta T_C + 1.8(3). \quad (7)$$

The obtained results using Eqs. 2 and 3 and Eqs. 3 and 7 have been collected in Table 1. A good agreement in both set of data can be observed once the contributions of low field are disregarded. Concerning ΔT_C, a constant value 12±2 K has been obtained for all the studied compounds. The existence of a transition distribution has already been reported in manganites. For example, for $La_{0.70-x}Eu_xSr_{0.30}MnO_3$ the existence of a chemical distribution has been reported because a partial substitution of Eu for La affects the magnetic and magnetocaloric properties of the compound [31]. In our samples, as ΔT_C shows no dependence on the Ni doping content, a chemical distribution can be discarded as responsible for the existence of the distribution of Curie temperatures. This distribution could be ascribed to the inhomogeneities and strains induced during the milling process, typical of the systems produced by this technique

[16] and which should be similar for all the samples studied in this work due to the equivalent milling conditions for all the compounds.

Concerning $\overline{T_C}$, the calculated values are significantly lower than those reported in the literature for the same compositions produced via auto-combustion method [8] and sol-gel method [9]. However, similar results have been found for $La_{0.7}Ca_{0.2}Ba_{0.1}MnO_3$ manganite powders (T_C = 297 K and 230 K for samples synthesized using a solid state reaction and high energy ball milling method, respectively [12]). The Curie temperature of $La_{0.78}Dy_{0.02}Ca_{0.2}MnO_3$ compound produced by ball-milling is also lower than those produced by a solid-state route and sol-gel method [13]. Moreover, milling process can generate iron impurities from the milling media, affecting the magnetic properties of the materials. In this sense, it has been reported a decrease of the Curie temperature with increasing Fe-content in manganites [32, 33].

For doped samples, it has been reported a decrease of T_C as Ni content increases [7, 8, 34, 35]. Generally, this decrease has been associated to an enhanced antiferromagnetic coupling between Ni^{2+}-O-Ni^{2+}, Mn^{4+}-O-Mn^{4+} and Mn^{3+}-O-Ni^{2+} with the increase of Ni^{2+} doping [36]. The double-exchange and superexchange interactions in manganites depend on the type and level of doping, the synthesizing technique and the processing method. The slight increase observed in $\overline{T_C}$ as Ni content increases could be explained by the modification in the strength of the ferro and antiferromagnetic interactions between Mn atoms and Mn and Ni atoms when added Ni atoms are introduced into the crystal structure.

Finally, some words are needed to analyze the low field behavior of the studied samples which deviates from Weiss model predictions. These results suggest the competition of the antiferro and ferromagnetic contributions at low fields, that strongly affect the

magnetization and the magnetic entropy change curves. The presence of these antiferromagnetic interactions at low magnetic fields are disregarded in the analysis of the law of approach to saturation by using high enough magnetic fields. Furthermore, other source of antiferromagnetic interactions in the studied samples have been detected, traces of β-MnO_2, which antiferromagnetic transition occurs at 92 K [37]. In fact, recent researches have shown that the magnetic moment of antiferromagnets can be controlled similarly to ferromagnets applying an external magnetic field that exceeds a certain value [38, 39]. Moreover, it has been shown that the balance between ferro and antiferromagnetic interactions in manganites can be tuned applying a pressure [40].

4. CONCLUSIONS

The magnetic and magnetocaloric properties of nanocrystalline $La_{0.7}Ca_{0.3}Mn_{1-x}Ni_xO_3$ (x = 0, 0.02, 0.07, 0.10) manganites produced by ball milling are experimentally studied. The formation of the perovskite structure has been verified using X-ray diffraction. The second order nature of the magnetic transition of the samples, analyzed by the Banerjee's criterion and the field dependence of the magnetic entropy change, was ascribed to the nanometric mean size of the particles (∼15 nm).

The milling process enhances the integration of the oxide powders in the perovskite structure. However, some traces of the MnO_2 phase were found. The antiferromagnetic character of this phase and the structural distortion of samples leads to a competing character of the ferromagnetic and antiferromagnetic interactions in the compounds at low fields.

The structural distortion produced by ball milling induces the existence of a distribution of Curie temperatures, which parameters have been determined in the frame of the

Weiss model. Comparison of experimental and simulated data allows us to confirm the reliability of the parameters of the distribution obtained from the analysis of the high field behaviour (approach to saturation and MCE from minimum field of 1 T). A slight increase of the average Curie temperature is observed as the Ni content increases, while the broadening of the distribution is constant for all the studied compounds.

Acknowledgements

This work was supported by AEI/FEDER-UE (Project MAT 2016-77265-R and Project US-1260179) and the PAI of the Regional Government of Andalucía. A.F. Manchón-Gordón acknowledges a VPPI-US fellowship. A. Gómez acknowledges the financial support of the Postgraduate Iberoamerican University Association (AUIP), Andalucian and Iberoamerican movement 2017 grant to visit the Dpto. de Física de la Materia Condensada, Universidad de Sevilla (Spain).

Data Availability

The raw/processed data required to reproduce these findings cannot be shared at this time as the data also forms part of an ongoing study.

Journal of Alloys and Compounds, 848 (2020) 156566.
https://doi.org/10.1016/j.jallcom.2020.156566

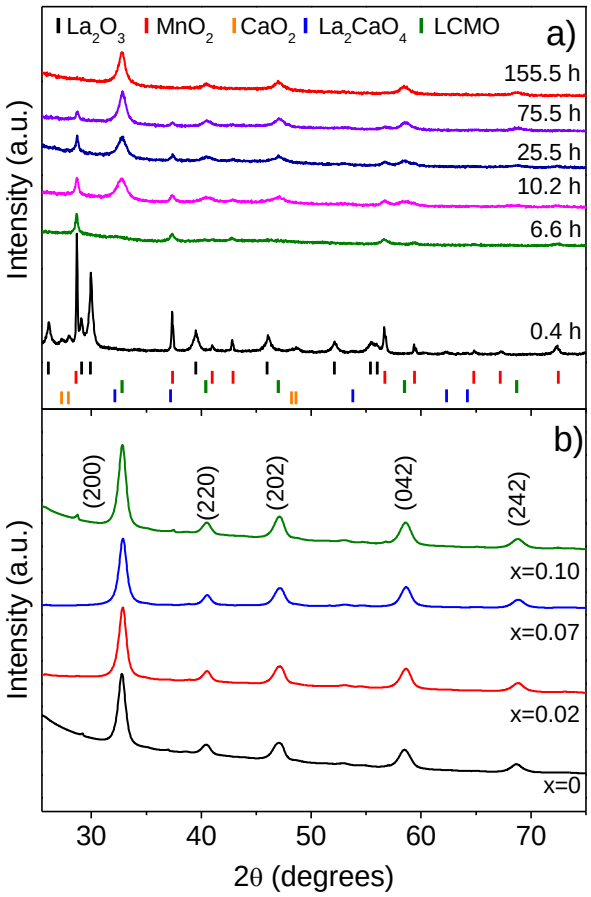

Figure 1. XRD patterns for $La_{0.7}Ca_{0.3}Mn_{1-x}Ni_xO_3$ for a) x=0 after selected equivalent milling times (marks identify the diffraction maxima of the different phases) and b) x=0, x=0.02, x=0.07 and x=0.10 at t_{eq}=155.5 h.

Journal of Alloys and Compounds, 848 (2020) 156566.
https://doi.org/10.1016/j.jallcom.2020.156566

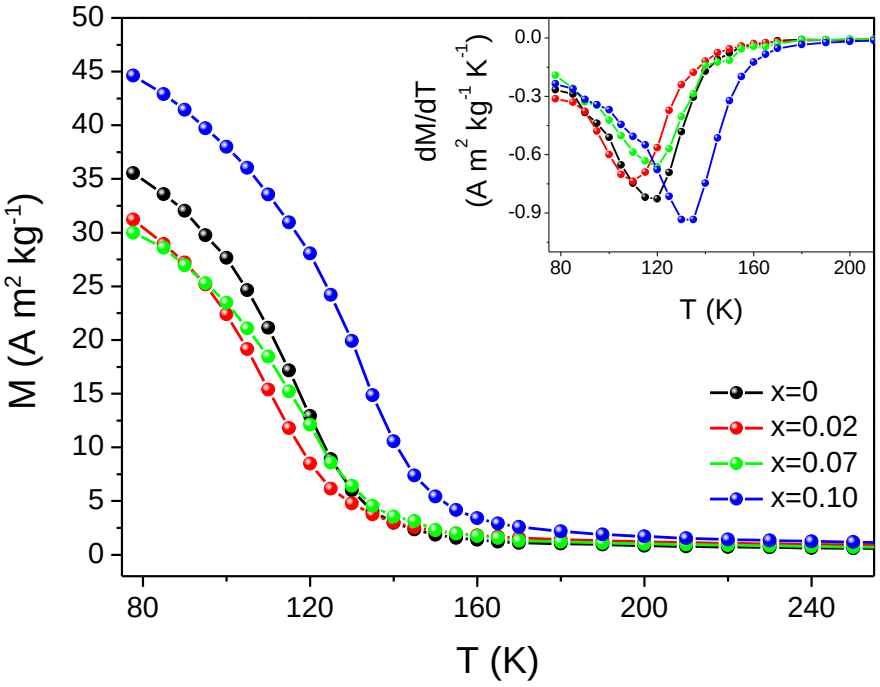

Figure 2. $M(T)$ at 0.1 T of the $La_{0.7}Ca_{0.3}Mn_{1-x}Ni_xO_3$ (x=0, 0.02, 0.07 and 0.10) samples at t_{eq}=155.5 h. Inset shows experimental data for dM/dT.

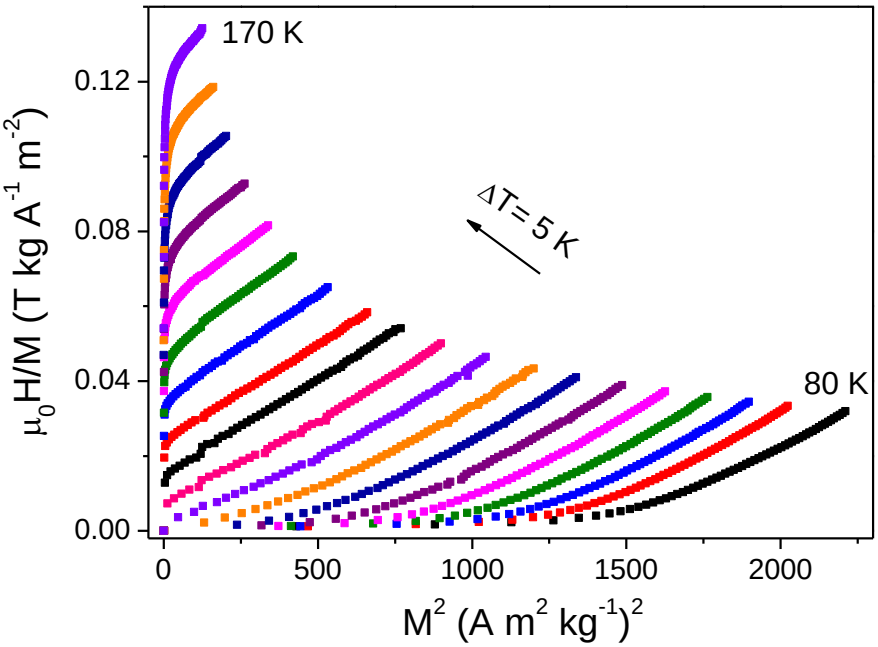

Figure 3. Arrott plots for temperatures close to the transition for the undoped sample at t_{eq}=155.5 h

Journal of Alloys and Compounds, 848 (2020) 156566.
https://doi.org/10.1016/j.jallcom.2020.156566

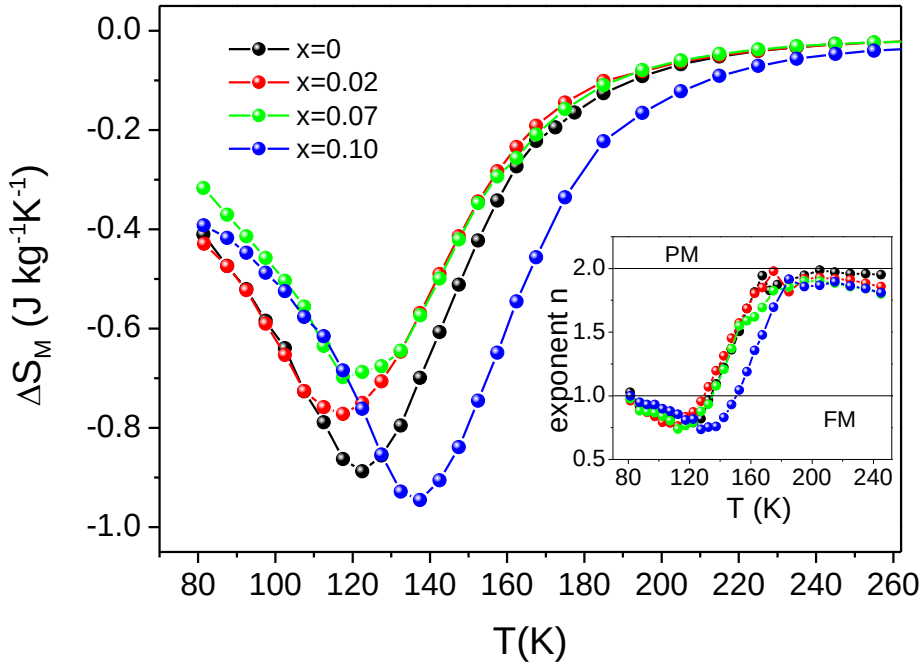

Figure 4. Magnetic entropy changes from zero field up to 1.5 T for $La_{0.7}Ca_{0.3}Mn_{1-x}Ni_xO_3$ samples (x=0, 0.02, 0.07 and 0.10) at t_{eq}=155.5 h. Inset: Corresponding exponent n. Lines are a guide to the eye.

Journal of Alloys and Compounds, 848 (2020) 156566.
https://doi.org/10.1016/j.jallcom.2020.156566

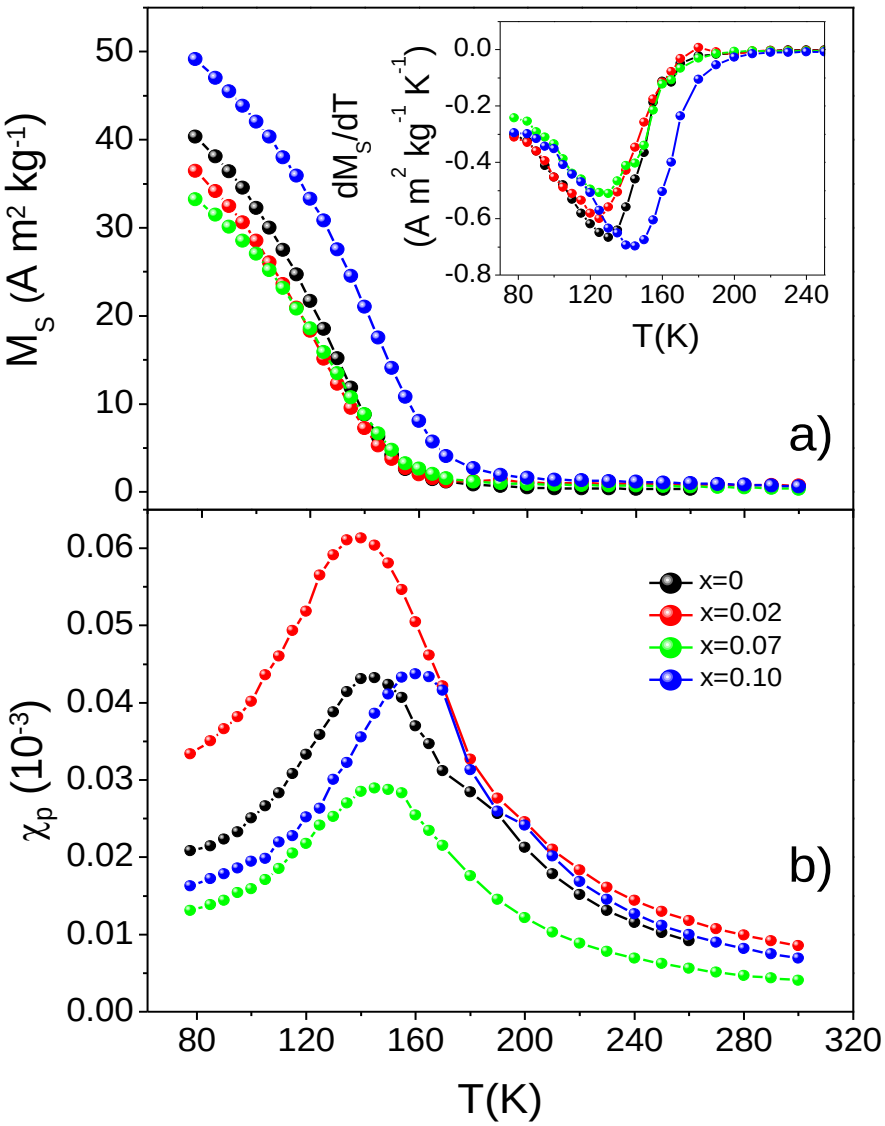

Figure 5. Temperature dependence of a) saturation magnetization and b) paramagnetic susceptibility curves from the law of approach to saturation for $La_{0.7}Ca_{0.3}Mn_{1-x}Ni_xO_3$ samples (x=0, 0.02, 0.07 and 0.10) at t_{eq}=155.5 h. Inset of the upper panel shows experimental data for dM_S/dT.

Journal of Alloys and Compounds, 848 (2020) 156566.
https://doi.org/10.1016/j.jallcom.2020.156566

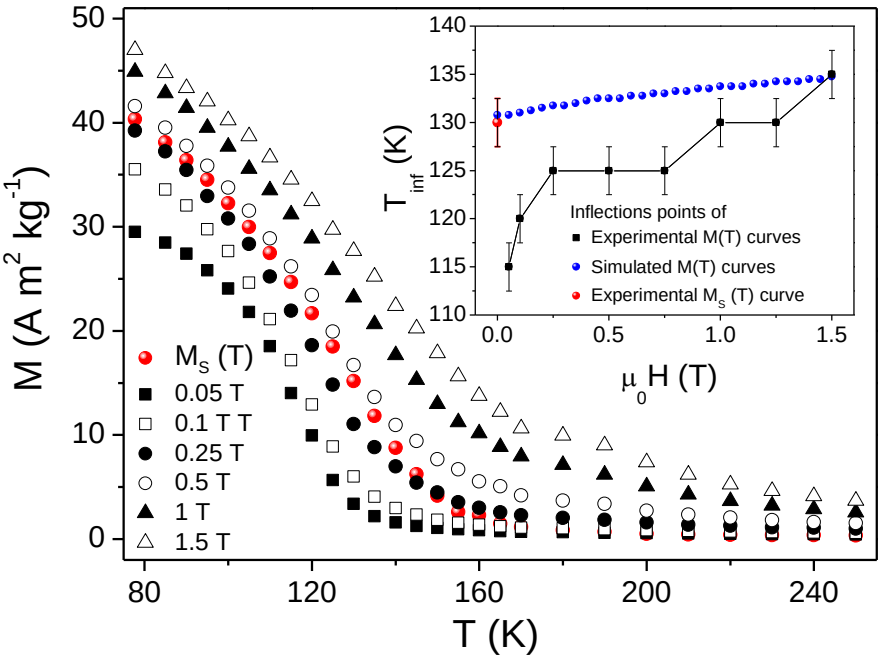

Figure 6. $M(T)$ of the undoped sample at t_{eq}=155.5 h and the indicated magnetic fields. $M_S(T)$ obtained from the law of approach to saturation is also displayed. Inset shows the inflection points $T_{inf}^{H}(H)$ of the $M(T)$ curves as a function of the magnetic field (black squares) and the simulated curves in the frame of the Weiss model assuming a Gaussian distribution with ΔT_C=12 K and $\overline{T_C}$=140 K. The red point at 0 T corresponds to the inflection point of the approach to saturation curve.

Journal of Alloys and Compounds, 848 (2020) 156566.
https://doi.org/10.1016/j.jallcom.2020.156566

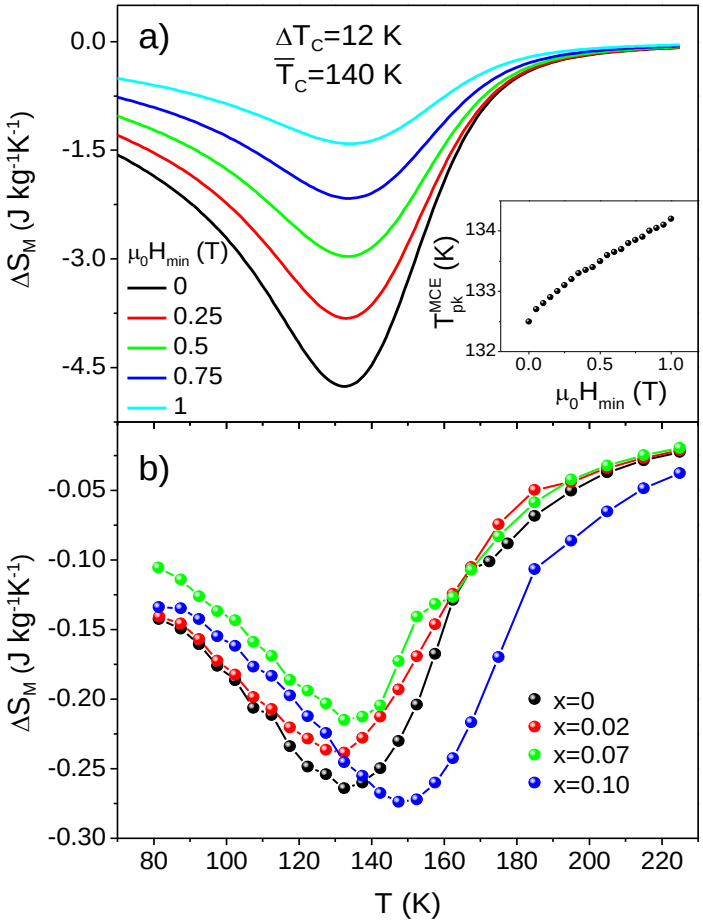

Figure 7. a) Simulated magnetic entropy change curves assuming a mean field approach based on the Brillouin function at different increment of magnetic field with ΔT_C=12 K and $\overline{T_C}$=140 K. The minimum magnetic field H_{min} has been modified and the maximum magnetic field $\mu_0 H_{max}$=1.5 T has remained constant. Inset shows the T_{pk}^{MCE} as a function of H_{min}. b) Experimental magnetic entropy change at $\mu_0 \Delta H$=0.5 T ($\mu_0 H_{min}$=1 T) for $La_{0.7}Ca_{0.3}Mn_{1-x}Ni_xO_3$ (x=0, 0.02, 0.07 and 0.1) samples at t_{eq}=155.5 h.

Journal of Alloys and Compounds, 848 (2020) 156566.
https://doi.org/10.1016/j.jallcom.2020.156566

Table 1. Experimental values of temperatures corresponding to the peaks of paramagnetic susceptibility T_{pk}^{χ}, the maximum of the magnetic entropy change T_{pk}^{MCE} from 1 to 1.5 T and the inflection point T_{inf} of the magnetization along with the average value of the Curie temperature $\overline{T_C}$ and the width of the distribution ΔT_C obtained by Eqs. 2 and 3 (superindex *inf*) and Eqs. 3 and 7 (superindex *MCE*) for different Ni content.

Ni-doping level (x)	T_{pk}^{χ} **(±3K)**	T_{inf} **(±3K)**	T_{pk}^{MCE} ($\mu_0 H_{min}$=1 T) **(±3K)**	$\overline{T_C}^{inf}$ **(±3K)**	$\Delta T_C{}^{inf}$ **(±2K)**	$\overline{T_C}^{MCE}$ **(±3K)**	$\Delta T_C{}^{MCE}$ **(±2K)**
0	145	130	133	139	12	139	12
0.02	140	125	128	134	12	134	12
0.07	145	130	133	139	12	139	12
0.10	160.0	145	148	154	12	154	12

Journal of Alloys and Compounds, 848 (2020) 156566.
https://doi.org/10.1016/j.jallcom.2020.156566

REFERENCES

[1] Franco V, Blazquez JS, Ipus JJ, Law JY, Moreno-Ramírez LM, Conde A. Magnetocaloric effect: from materials research to refrigeration devices. Progress in Materials Science 2018;93:112-232. https://doi.org/10.1016/j.pmatsci.2017.10.005

[2] Gschneidner KA, Pecharsky VK, Tsokol AO. Recent developments in magnetocaloric materials. Reports on Progress in Physics 2005;68:1479-539. https://doi.org/10.1088/0034-4885/68/6/R04

[3] Phan MH, Yu SC. Review of the magnetocaloric effect in manganite materials. Journal of Magnetism and Magnetic Materials 2007;308:325-40. https://doi.org/10.1016/j.jmmm.2006.07.025

[4] Goodenough J, Arnott RJ, Menyuk N, Wold A. Relationship between crystal symmetry and magnetic properties of ionic compounds containing Mn^{3+}. Physical Review 1961;124:373-84. https://doi.org/10.1103/PhysRev.124.373

[5] Zener C. Interaction between the d-shells in the transition metals .2. ferromagnetic compounds of manganese with perovskite structure. Physical Review 1951;82:403-5. https://doi.org/10.1103/PhysRev.82.403

[6] Eshraghi M, Salamati H, Kameli P. The effect of NiO doping on the structure, magnetic and magnetotransport properties of $La_{0.8}Sr_{0.2}MnO_3$ composite. Journal of Alloys and Compounds 2007;437:22-6. https://doi.org/10.1016/j.jallcom.2006.07.104

[7] Yadav A, Shah J, Gupta R, Shukla A, Singh S, Kotnala RK. Role of spin-glass phase for magnetoresistance enhancement in nickel substituted lanthanum calcium manganite. Ceramics International 2016;42:12630-8. https://doi.org/10.1016/j.ceramint.2016.04.162

[8] Gomez A, Chavarriaga E, Supelano I, Parra CA, Moran O. Tuning the magnetocaloric properties of $La_{0.7}Ca_{0.3}MnO_3$ manganites through Ni-doping. Physics Letters A 2018;382:911-9. https://doi.org/10.1016/j.physleta.2018.01.030

[9] Laajimi K, Khlifi M, Hlil EK, Gazzah MH, Dhahri J. Enhancement of magnetocaloric effect by Nickel substitution in $La_{0.67}Ca_{0.33}Mn_{0.98}Ni_{0.02}O_3$ manganite oxide. Journal of Magnetism and Magnetic Materials 2019;491:165625. https://doi.org/10.1016/j.jmmm.2019.165625

[10] Zener C. Interaction between the d-shells in the transition metals. Physical Review 1951;81:440-4. https://doi.org/10.1103/PhysRev.82.403

[11] Mahjoub S, Baazaoui M, Hlil EK, Oumezzine M. Effect of synthesis techniques on structural, magnetocaloric and critical behavior of $Pr_{0.6}Ca_{0.1}Sr_{0.3}Mn_{0.975}Fe_{0.025}O_3$ manganites. Ceramics International 2015;41:12407-16. https://doi.org/10.1016/j.ceramint.2015.06.078

[12] Ezaami A, Sellami-Jmal E, Chaaba I, Cheikhrouhou-Koubaa W, Cheikhrouhou A, Hlil EK. Effect of elaborating method on magnetocaloric properties of $La_{0.7}Ca_{0.2}Ba_{0.1}MnO_3$ manganite. Journal of Alloys and Compounds 2016;685:710-9. https://doi.org/10.1016/j.jallcom.2016.05.332

[13] Riahi K, Messaoui I, Cheikhrouhou-Koubaa W, Mercone S, Leridon B, Koubaa M, Cheikhrouhou A. Effect of synthesis route on the structural, magnetic and magnetocaloric properties of $La_{0.78}Dy_{0.02}Ca_{0.2}MnO_3$ manganite: A comparison between sol-gel, high-energy ball-milling and solid state process. Journal of Alloys and Compounds 2016;688:1028-38. https://doi.org/10.1016/j.jallcom.2016.07.043

[14] Bolarin AM, Sanchez F, Palomares S, Aguilar JA, Torres-Villasenor G. Synthesis of calcium doped lanthanum manganite by mechanosynthesis. Journal of Alloys and Compounds 32007;436:335-40. https://doi.org/10.1016/j.jallcom.2006.07.061

[15] Messaoui I, Riahi K, Cheikhrouhou-Koubaa W, Koubaa M, Cheikhrouhou A, Hlil EK. Phenomenological model of the magnetocaloric effect on $Nd_{0.7}Ca_{0.15}Sr_{0.15}MnO_3$ compound prepared by ball milling method. Ceramics International 2016;42:6825-32. https://doi.org/10.1016/j.ceramint.2016.01.060

[16] Manchon-Gordon AF, Ipus JJ, Moreno-Ramirez LM, Blazquez JS, Conde CF, Franco V, Conde A. Correction of the shape effect on magnetic entropy change in ball milled $Fe_{70}Zr_{30}$

alloys. Journal of Alloys and Compounds 2018;765:437-43. https://doi.org/10.1016/j.jallcom.2018.06.176
[17] Alvarez-Alonso P, Llamazares JLS, Sanchez-Valdes CF, Cuello GJ, Franco V, Gorria P, Blanco JA. On the broadening of the magnetic entropy change due to Curie temperature distribution. Journal of Applied Physics 2014;115:17A929. https://doi.org/10.1063/1.4867346
[18] Manchon-Gordon AF, Lopez-Martin R, Vidal-Crespo A, Ipus JJ, Blazquez JS, Conde CF, Conde A. Distribution of Transition Temperatures in Magnetic Transformations: Sources, Effects and Procedures to Extract Information from Experimental Data. Metals 2020;10.2:226. https://doi.org/10.3390/met10020226
[19] Manchon-Gordon AF, Moreno-Ramirez LM, Ipus JJ, Blazquez JS, Conde CF, Franco V, Conde A. A procedure to obtain the parameters of Curie temperature distribution from thermomagnetic and magnetocaloric data. Journal of Non-Crystalline Solids 2019;520:119460. https://doi.org/10.1016/j.jnoncrysol.2019.119460
[20] Ipus JJ, Blazquez JS, Franco V, Millan M, Conde A, Oleszak D, Kulik T. An equivalent time approach for scaling the mechanical alloying processes. Intermetallics 2008;16:470-8.
[21] Coey JMD. Magnetism and magnetic material. New York: Cambridge University Press; 2010. https://doi.org/10.1016/j.intermet.2007.12.011
[22] http://www.lakeshore.com/products/Vibrating-Sample-Magnetometer/Pages/MCE.aspx.
[23] Tang W, Lu WJ, Luo X, Wang BS, Zhu XB, Song WH, Yang Z, Sun Y. Particle size effects on $La_{0.7}Ca_{0.3}MnO_3$: size-induced changes of magnetic phase transition order and magnetocaloric study. Journal of Magnetism and Magnetic Materials 2010;322:2360-8. https://doi.org/10.1016/j.jmmm.2010.02.038
[24] Waitz T, Karnthaler HP. Martensitic transformation of NiTi nanocrystals embedded in an amorphous matrix. Acta Materialia 2004;52:5461-9. https://doi.org/10.1016/j.actamat.2004.08.003
[25] Seki K, Kura H, Sato T, Taniyama T. Size dependence of martensite transformation temperature in ferromagnetic shape memory alloy FePd. Journal of Applied Physics 2008;103: 063910. https://doi.org/10.1063/1.2890143
[26] Manchon-Gordon A, Ipus JJ, Kowalczyk M, Wojcik A, Blazquez JS, Conde CF, Maziarz W, Svec Sr. P, Conde A. Effect of pressure on the phase stability and magnetostructural transitions in nickel-rich NiFeGa ribbons. Journal of Alloys and Compounds 2020;156092. https://doi.org/10.1016/j.jallcom.2020.156092
[27] Law JY, Franco V, Moreno-Ramirez LM, Conde A, Karpenkov DY, Radulov I, Skokov KP, Gutfleisch O. A quantitative criterion for determining the order of magnetic phase transitions using the magnetocaloric effect. Nature Communications 2018;9:2680. https://doi.org/10.1038/s41467-018-05111-w
[28] Franco V, Blazquez JS, Conde A. Field dependence of the magnetocaloric effect in materials with a second order phase transition: A master curve for the magnetic entropy change. Applied Physics Letters 2006;89:222512. https://doi.org/10.1063/1.2399361
[29] Moran O, Gomez A, Supelano I, Parra CA, Izquierdo JL. Assessment of the critical behavior near the FM to PM phase transition in nano-crystalline $La_{0.7}Ca_{0.3}Mn_{1-x}Ni_xO3$ (x=0, 0.02, 0.07, 0.10) samples synthesized by auto-combustion. Journal of Magnetism and Magnetic Materials 2019;477:22-6. https://doi.org/10.1016/j.jmmm.2019.01.046
[30] Taboada-Moreno CA, Sanchez-De Jesus F, Pedro-Garcia F, Cortes-Escobedo CA, Betancourt-Cantera JA, Ramirez-Cardona M, Bolarín-Miró AM. Large magnetocaloric effect near to room temperature in Sr doped $La_{0.7}Ca_{0.3}MnO_3$. Journal of Magnetism and Magnetic Materials 2020;496:165887. https://doi.org/10.1016/j.jmmm.2019.165887
[31] Amaral JS, Tavares PB, Reis MS, Araujo JP, Mendonca TM, Amaral VS, Vieira JM. The effect of chemical distribution on the magnetocaloric effect: A case study in second-order phase transition manganites. Journal of Non-Crystalline Solids 2008;354:5301-3. https://doi.org/10.1016/j.jnoncrysol.2008.05.078

Journal of Alloys and Compounds, 848 (2020) 156566.
https://doi.org/10.1016/j.jallcom.2020.156566

[32] Ho TA, Thanh TD, Ho TO, Phan MH, Phan TL, Yu SC. Magnetic properties and magnetocaloric effect in Fe-doped La0.6Ca0.4MnO3 with short-range ferromagnetic order. Journal of Applied Physics 2015;117:17A724 https://doi.org/10.1063/1.4915103
[33] Kumar MA, Mahato RN. Effect of Fe substitution on structural, magnetic and magnetocaloric properties of nanocrystalline $La_{0.7}Te_{0.3}Mn_{1-x}Fe_xO_3$ (x=0.1, 0.3). Physica B-Condensed Matter 2017;511:83-8. https://doi.org/10.1016/j.physb.2017.02.006
[34] Mohamed AMA, Hernando B, Ahmed AM. Magnetic, magnetocaloric and thermoelectric properties of nickel doped manganites. Journal of Alloys and Compounds 2017;692:381-7. https://doi.org/10.1016/j.jallcom.2016.09.050
[35] Hassayoun O, Baazaoui M, Laouyenne MR, Hosni F, Hlil EK, Oumezzine M, Farah Kh. Magnetocaloric effect and electron paramagnetic resonance studies of the transition from ferromagnetic to paramagnetic in $La_{0.8}Na_{0.2}Mn_{1-x}Ni_xO_3$ (0 <= x <= 0.06). Journal of Physics and Chemistry of Solids 2019;135:109058 https://doi.org/10.1016/j.jpcs.2019.06.006
[36] Reshmi CP, Pillai SS, Suresh KG, Varma MR. Room temperature magnetocaloric properties of Ni substituted $La_{0.67}Sr_{0.33}MnO_3$. Solid State Sciences 2013;19:130-5. https://doi.org/10.1016/j.solidstatesciences.2013.02.019
[37] Zhou CS, Wang JF, Liu X, Chen FY, Di YY, Gao SL, Shi Q. Magnetic and thermodynamic properties of alpha, beta, and gamma-MnO_2. New Journal of Chemistry 2018;42:8400-7. https://doi.org/10.1039/C8NJ00896E
[38] Marti X, Fina I, Jungwirth T. Prospect for Antiferromagnetic Spintronics. Ieee Transactions on Magnetics 2015;51.7109970. https://doi.org/10.1109/TMAG.2014.2358939
[39] Gomonay O, Jungwirth T, Sinova J. Concepts of antiferromagnetic spintronics. Physica Status Solidi-Rapid Research Letters 2017;11:1700022 https://doi.org/10.1002/pssr.201700022
[40] Vu MT, Kozlenko DP, Kichanov SE, Troyanchuk IO, Lukin EV, Khiem LH, Savenko BN. Pressure induced antiferromagnetism in the manganite $La_{0.7}Sr_{0.3}Mn_{0.83}Nb_{0.17}O_3$. Journal of Alloys and Compounds 2016;681:527-31 https://doi.org/10.1016/j.jallcom.2016.04.180